Contents list available at IJRED website

Int. Journal of Renewable Energy Development (IJRED)

Journal homepage: http://ejournal.undip.ac.id/index.php/ijred

Evaluating the Potential Energy of a Heliostat Field and Solar Receiver of Solar Tower Power Plants in the Southern Region of Turkey

Ra'ad K Mohammed Aldulaimi[a,b1 *] and Mehmet Sait Söylemez[a]

[a] *Department of Mechanical Engineering, University of Gaziantep, 27310 Gaziantep, Turkey*

[b] *University of Baghdad, Baghdad, Iraq*

ABSTRACT. A prior study on the performance of high-efficient models for a heliostat field and solar receiver at various candidate locations (e.g., certain regions in the south of Turkey) helped determine suitable locations for installing solar tower power plant units. This study considered the fact that solar tower power plants are affected by the working conditions of a particular site, which helps realize the highest performance of the solar power tower plant. An optimized heliostat field consisting of 2650 SENER heliostats and a model of a solar receiver based on the data obtained using Gemasolar in Seville, Spain, was used as a reference in this work. Each heliostat position is specified using an optimization algorithm that refines previously proposed models, and two parameters are added to this model to further optimize the heliostat layout. Then, a sample analytical thermal model is used for predicting the radiative and convective heat losses from the receiver system.

***Keywords*:** heliostat field, simulation, solar power tower plant, solar receiver, Turkey

Article History: Received March 13rd 2016; Received in revised form Jun 22nd 2016; Accepted July 3rd 2016; Available online
How to Cite This Article: Ra'ad, K, M, A. and Mehmet, S, S. (2016), Evaluating the potential energy of a heliostat field and solar receiver of solar tower power plants in the southern region of Turkey. *Int. Journal of Renewable Energy Development, 5*(2), 151-161, http://dx.doi.org/10.14710/ijred.5.2.151-161

1. Introduction

The increase in energy demand, the depletion of fossil fuels, and the awareness of the public on environmental problems motivate the generation of electrical energy from renewable sources. Sunshine is the most abundant source of energy on Earth, and every year, the sun delivers more than 10,000 times the amount of energy required by humans for their daily use (Chiesi 2013). Among all the technologies for concentrated solar power (CSP), the use of solar power tower plants (SPTPs) is unique for achieving highly focused solar radiation on a large scale, for generating electrical power (Siala 2001). SPTPs use several hundred or even thousands of reflectors, called heliostats, as intermediate optical devices between the sun's rays and an energy absorbing device. Heliostats are set around a receiver that follows the sun, and the reflection of the light from the sun further focuses it up to 1000 times to a central receiver placed at the central point at the top of a high tower. A computer controls each heliostat's rotation around two axes to ensure light is continuously directed correctly, with a tracking error of less than a fraction of a degree. By this orientation, the intensified sunlight is focused directly on the tower receiver, where an absorber is heated to temperatures of approximately 1000 °C or more (Leonardi 2011). A heat transfer fluid (HTF) then transfers the absorbed energy to a heat exchanger connected to a gas or steam turbine, which is in turn coupled to an electric generator.

The main factor in this system as well as the topic of many studies is the ideal layout of the reflector field and the ideal design of the solar receiver, mainly because the approach requires 50% of the full price of the scheme for heliostat field (Wei 2010) and 19% of the full price of the scheme for receiver (Kolb 2011), and the annual energy

[1] * Corresponding author:
Email: rd13434@mail2.gantep.edu.tr,
eng.raadalduleimi@gmail.com, eng_raadalduleimi@yahoo.com

loss in the heliostat field is approximately 47% (Wei 2010). Several codes have been produced since the 70s for estimating ideal layouts; and most of those codes are presented in (Garcia 2008). For the most part, the most recent codes (Chiesi 2013, Noone 2012, Collado, 2013, Besarati 2014) identify various forms of access to increase the global optical efficiency (η), which the present study depends on, to estimate the optical performance of the field. The main purpose of this work is to apply software simulations, a dynamic simulation developed in MATLAB, and consider all average days in the year, as presented in (American Society of Heating, Refrigeration, and Air-conditioning Engineers) (ASHRAE 2013), within a specified interval time, to study the potential of SPTP technology through a hypothetical relocation of Seville, Spain's Gemasolar SPTP to regions in the south of Turkey (Gaziantep, Sanliurfa, and Finike). This study also determines where the highest energy output can be achieved by comparing the performance in terms of the accumulated energies and efficiencies of main units that are affected by special construction requirements in these border locations.

Further, the field and geometrical data receiver model for a GEMASOLAR (SPTP) (Seville –Spain), which is a modern, efficient, and highly productive energy plant, with its border location is considered as a reference in this study. GEMASOLAR is 20 MW power plant that was established in 2011 (Burgaleta 2011). One of the reasons this plant is successful and possesses distinct characteristics is because of the careful selection of the site. It is situated within the city limits of Fuentes de Andalucía in the province of Seville, Spain, which is considered to be one of the most sunniest and warmest areas in the Europe. It is considered as a reference case in several studies. For instance, Amadei (2013) studied the hypothetical relocation of the same plant to different Chinese regions through software simulation (Solar Advisor Model, SAM). Collado (2013) also studied the optimization of the heliostat field by adopting radially staggered distribution with an implemented Campo code, and estimated the maximum annual energy with a new layout suggested. In the present study, each mirror position is specified by utilizing the layouts of the MIT team model (Noone 2012), while two parameters of this model settle down the layout outline of the reflectors, estimated by used an optimization algorithm. Then, the thermal performance of the receiver is estimated using a simple analytical model.

2. Simulation Tools

2.1. Optical efficiency factors

The optical efficiency, which is a function of the energy losses associated with the heliostat field, is given in Eq. (1):

$$\eta = \eta_{ref} \times \eta_{cos} \times \eta_{at} \times \eta_{in} \times \eta_{s\&b} \quad (1)$$

where η_{ref} represents the reflectivity of the heliostats, η_{cos} represents the cosine of the incidence angle between the sun rays and the heliostat normal, η_{at} represents the atmospheric attenuation efficiency, which accounts for radiation losses in the distance (D) between a heliostat and the receiver and can be estimated by Eqs. 2 and 3, as given in Refs (Noone 2012, Collado 2013):

$$\eta_{at} = 0.99321 - 0.000176D + 1.97 \times 10^{-8}D^2 \qquad D \leq 1000m \quad (2)$$

$$\eta_{at} = e^{-0.0001106D} \qquad D > 1000m \quad (3)$$

η_{in} represents the interception efficiency, which is related to the energy directed to the receiver that does not fall on the absorbing area, because the reflector surface accuracy, beam spread, mirror canting accuracy, and tracking accuracy all have a major effect on the flux distribution at the receiver. An analytical flux density model or the HFLCAL model presented by Collado (2013), Schmitz (2006) and Collado (2010) which are simple and accurate tools applied to estimate the ($\boldsymbol{\eta_{in}}$) and flux distribution, are used in this study. The HFLCAL model integrated the flux distribution along an absorbing surface of the receiver to obtain the intercepted power at a certain point in time, as given by Eq. 4

$$\eta_{in} = \frac{1}{2\pi\sigma_{tot}^2}\int_{(x_r)}\int_{(y_r)} e^{\left(-\frac{x_r^2+y_r^2}{2\sigma_{tot}^2}\right)} dy_r\, dx_r \quad (4)$$

(σ_{tot}) is the total dispersion of the flux distribution and is expressed by Eq 5. The coordinates x_r and y_r are related to the vertical plane of the receiver with the origin as the center (the aim point).

$$\sigma_{tot} = \sqrt{D^2\left(\sigma_{sun}^2 + \sigma_{bq}^2 + \sigma_{ast}^2 + \sigma_t^2\right)}/\sqrt{\cos rec} \quad (5)$$

where $(\sigma_{sun}, \sigma_{bq}, \sigma_{ast}, \sigma_t)$ represent the sun shape error, beam quality, the astigmatic effect, and the tracking error, respectively. Further ($\cos rec$) is the incidence cosine of the reflected central ray from the heliostat on the receiver surface (a vertical plane). Further details about the HFLCAL functions and constants value can be found in Collado (2013). $\eta_{s\&b}$ represents the shading and blocking efficiency. Shading occurs when a heliostat is shaded from sunlight by an adjoining heliostat or a tower, and similarly blocking occurs if a heliostat block the sun rays reflected from an adjoining to the receiver, In this study, the central ray tracing and discretization technique, which is presented in Ref. (Noone 2012), was adapted to calculate

the ($\boldsymbol{\eta_{s\&b}}$) with small subdivisions (100 elements) and high accuracy.

On the other hand, because any SPTP optimization operation should depend on the annual energy estimation of each different layout, the insolation-weighted mean yearly heliostat field efficiency ($\eta_{year,Eb}$) was calculated in Refs (Noone 2012, Besarati 2014) using Eq. (6):

$$\eta_{year,Eb} = \frac{\sum_{day=1}^{365} \int_{sunrise}^{sunset} E_b(t)\eta(t)dt}{\sum_{day=1}^{365} \int_{sunrise}^{sunset} E_b(t)dt} \qquad (6)$$

To compromise between the CPU time and resolution, specify the 21st of each month during the year (average day), and carry out over all days the same Eq. (6) with all computations that are related to the other parameters of optical efficiency (Besarati 2014).

2.2 Solar radiation

The annual energy from the receiver is the sum of the instantaneous energies produced by the heliostat field (Collado 2013). The solar radiation along time increments are sampled from the American Society of Heating, Refrigeration, and Air-conditioning Engineers (ASHRAE) clear-sky radiation model (ASHRAE 2013) and utilizing two monthly factors; the relative air mass(m) can be estimated by Eq. (7):

$$m = \frac{1}{\sin\alpha + 0.50572(6.07995 + \alpha)^{-1,6364}} \quad (7)$$

where (α) represents the solar altitude angle and is expressed in degrees. The beam normal radiation E_b is given by Eq. (8):

$$E_b(t) = E_o exp[-\tau_b m^b] \qquad (w/m^2) \qquad (8)$$

in which the beam's air mass exponents b are given by Eq. (9):

$$b = 1.219 - 0.043\tau_b - 0.151\tau_d - 0.204\tau_b\tau_d \qquad (9)$$

and E_o is the extraterrestrial normal irradiance accumulated following Eq. (10):

$$E_o = E_{sc}\left(1 + 0.033cos\left(360^o \frac{(n_d-3)}{365}\right)\right) \qquad (w/m^2) \ (10)$$

In Eq. (10), E_{sc} is equal to 1366.1 W/m^2, n_d is the day number, and τ_b and τ_d represent the apparent beam and diffusion optical depths, respectively, which are site specific and change during the year. For Seville, Spain, and other cities that study SPTP technology, these last parameters are given in (ASHRAE 2013) for each city on the 21st day of each month.

2.3 Ambient temperature (°C)

The procedures for generating 24-h temperature data sequences, as in (ASHRAE 2013) are suitable inputs to the thermal equations describing the receiver, are based on three factors: the monthly dry bulb design temperature (DB), the mean daily DB temperature range (MCDBR), and fractions of the daily temperature range. These are included in (ASHRAE 2013) for the 21st day of each month for Seville, Spain, (Lat: 37.42) and other cities, except for the fractions of the daily temperature range because it is a function of solar time and is therefore tabulated for each 24 h of solar time. To calculate the hourly temperature T_{amb}, the fraction of the DB daily range is subtracted from the dry bulb monthly design temperature as presented in Eq. (11):

$$T_{amb} = (DB) - \left(fraction\ of\ daily\ temperature\ range \times (MCDBR)\right) \qquad (11)$$

2.4 Heliostat and receiver specifications

Gemasolar, an SPTP in Seville, Spain, is the plant used as a reference in this work. The complete dimensions of the SENER heliostats used in Gemasolar are presented in (Collado 2013, Burgaleta 2011, Amadei 2013); the field parameters used in this study are presented in Table 1 along with other parameters of the receiver model, which are considered similar to those of Gemasolar, because some data related to the receiver model is hard to obtain, therefore, the study depended on some parameters from the literature review of solar two (Pacheco 2002), as the number of panels and the tube wall thickness, which considered (24, 1.25mm) respectively and the number of path flow for HTF (2), and set the number of tubes n_t in each panel which equal 38.

Table 1.
Gemasolar field and receiver parameters (Collado 2013, Burgaleta 2011, Amadei 2013)

Heliostats	
Width $\boldsymbol{W_h}$ **(m)**	12.305
Height $\boldsymbol{H_h}$ **(m)**	9.752
Heliostat total diagonal, $\boldsymbol{d_h}$ **(m)**	15.7
Heliostat total area, $\boldsymbol{A_h}$ **(m²)**	120
Heliostat mirror area, $\boldsymbol{A_m}$ **(m²)**	115.7
Effective reflectivity, $\boldsymbol{\eta_{ref}}$	0.88 × 0.95
Heliostat numbers	2650
Receiver	
Tower optical height $\boldsymbol{h_t}$ **(m)**	140
Receiver radius $\boldsymbol{R_r}$ **(m)**	4
Receiver height $\boldsymbol{H_r}$ **(m)**	9
Coating absorptance	0.95
Max receiver flux (kw_t/m^2)	1000
Inlet Temp for HTF $\boldsymbol{T_{HTF,in}}$ (°C)	290
Outlet Temp for HTF $\boldsymbol{T_{HTF,ou}}$ (°C)	595

2.5 Coordinate system

In the selection coordinate system (referred to in the following text as "tower system of coordinates"), east is in the positive (y) direction, north is in the positive (z) direction, and the zenith is in the (x) direction, as shown in Fig. (1).

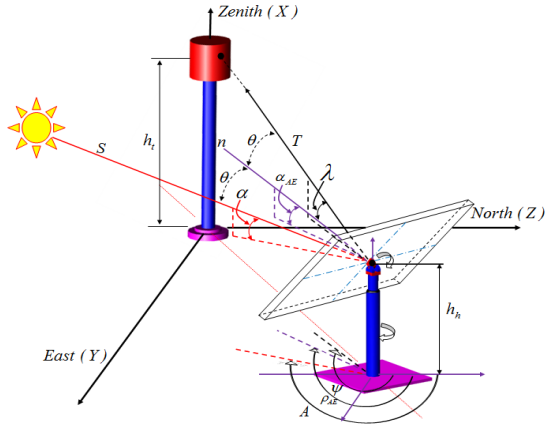

Fig. 1 System Coordinate for heliostat fields and receiver

Given that the sun is a moving object while the receiver is a fixed object, the normal (n) of the heliostat has to be adjusted when the sun position changes with time to ensure that the heliostat is oriented at the necessary angles.

The incident angle on the heliostat (θ) Similar to the angle of reflection, as indicated by Snell's law of reflection, therefore, the bisector of (s) and (T) is the heliostat normal (n), as shown in Eq. (12):

$$n = \frac{s + T}{|s + T|} \qquad (12)$$

The unit vector (s) refers to the sun and it is estimated as presented in Ref. (Duffie 1991) depending upon the solar altitude angle (α) and solar azimuth angle (A). The unit vector (T) is directed toward the aim point (receiver). Thus, the vector (T) is in the direction of the central reflected ray.

To determine the (η) of the heliostat, the heliostat position frame should be estimated. The altered orientation of the frame during the sun tracking period in three-dimensional space can be modeled by applying the coordinate transformation, which is presented in Ref. (Stine 1985). The rest position or the initial coordinate of the frame is first defined in a fixed coordinate system. When the plane of the heliostat is parallel to the x-y plane, the normal to its surface(n) is directed to the north direction. The reflector is oriented using an actuator for rotation in the coordinate transformation for the azimuth-elevation ***(AE)*** sun-tracking method, as presented in Ref. (Chong 2011). The first rotation transformation by the angle (α_{AE}) about the Y-axis will transform the point from the fixed coordinate system to an elevation-movement coordinate system. The second rotation transformation for the rotational movement by the angle (ρ_{AE}) about the X-axis will transform the point of the elevation-movement coordinate system to an azimuth-movement coordinate system,

3. Mathematical Model for Heliostat Field Layout

The positioning of the heliostats around the tower is an essential step that depends on many factors. On the other hand, the annual optical efficiency is considered to be the main factor for evaluating different field layouts.

First, the layout of the heliostat field and the position for each heliostat are defined based on the model presented in (Noone 2012), which was inspired by the spiral patterns of the phyllotaxis disc. This layout was shown to increase the overall efficiency and is expressed by Eqs. (13) and (14), as presented in (Noone 2012):

$$\theta_{hp} = 2\pi\varphi^{-2}n_h \qquad (13)$$

$$r_{hp} = an_h^b \qquad (14)$$

where θ_{hp} represents the polar position angle for heliostats in the field, r_{hp} represents the radial position of the heliostat, and a and b represent the field layout design variables. From Eqs. (13) and (14), evaluations of the different layouts are verified by forming various layout distributions with adjustments to the a and b parameters, using an optimization algorithm to estimate the ideal a and b values. The limits of a and b are assumed to be [2, 8] and [0.4, 0.7], respectively. A feature of the created heliostat field should be larger than the heliostat number for the necessary range. Therefore, this study started with 5000 heliostats, with the objective of restricting the field to determine the optimal layout of 2650 heliostats.

The field size was selected to include 2650 heliostats, which have the highest $\eta_{year,Eb}$from 5000 heliostats, for comparison with the case study model. The distance between the heliostat and its neighbors is the main condition that must be specified before optimizing the field, to prevent overlap among the close circles in which the heliostats move. Therefore, a program was written such that layouts that lead to interference between the circle movements for the heliostats were not considered. Furthermore, the diagonal of the total reflector area d_h equals 15.7 m for SENER heliostats (see Table 1), and the proposed code does not consider any extra separation distance (d_{sep} = 0).

In this study, a genetic algorithm (GA) is used to implement the necessary optimization duty because GA is one of the most efficient optimization methods.
Successive random values of the design variables are input until the highest value of $\boldsymbol{\eta_{year,Eb}}$ is recorded; in this case, the a and b parameters were 3.55 and 0.675, respectively, corresponding to a layout with 2650 heliostats.
However, the present value of $\eta_{year,Eb}$ results are shown in Fig. (2), which are based on the new values of the specified a and b parameters that are compared with other values of the same parameters in other studies (Noone 2012) and (Besarati 2014), which used the same heliostat area and layout. The results show that a higher performance was obtained than others with new values of parameters, as shown in Table (2).

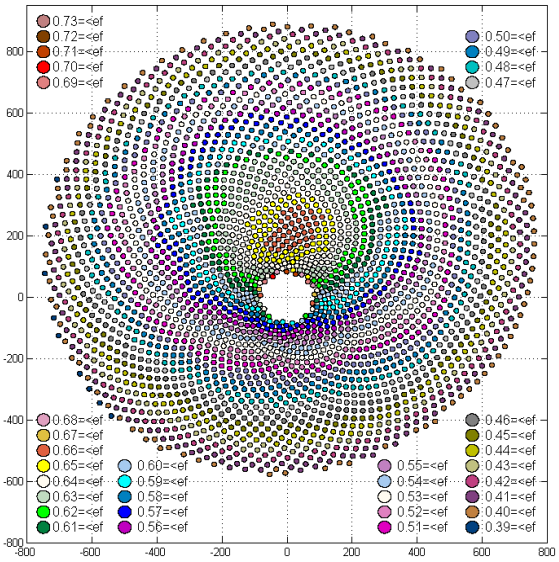

Fig. 2. Layout of the field and $(\eta_{year,Eb})$ for each heliostat

Table 2:
Yearly weighted efficiency for different design variables

	$a = 3.55$ b = 0.675 present model	$a = 4.5$ b = 0.65 (Noone 2012)	$a = 3.935$ b = 0.70 (Besarati 2014)
$\eta_{year,Eb}$	52.8589%	51.7604%	48.563%

In order to increase the reliability, implement the same value of the parameters of Ref. (Noone 2012), with same number of heliostats and locations. The results of unweighted heliostat field efficiency are obtained with the same Eq. (6), but without considering $E_b(t)$ in the computation; the result obtained in Ref . (Noone 2012) is 64.3% and that obtained in the present study is 65.173%.

The second comparison is targeted by computing the value of the field efficiency in GEMASOLAR by the modeling results of Ref. (Collado 2013), depending on the same reference data and considering the same model of solar radiation and same duration of simulation in Ref. (Collado 2013). The comparison shows that the result (57.3693%) is very close to the published data of Ref. (Collado 2013), which is (57.232%).

4. Energy Balance Model of Solar Receiver

In an SPTP, the receiver is the heat exchanger that intercepts the concentrated sunlight and discharges its energy to an HTF, which may be water, molten salt, atmospheric air, or pressurized air. The solar receiver should act like a blackbody by minimizing radiation losses. The model presented in this paper is based on molten salt tubular cylindrical receivers, and the characteristics of this model is presented in Table (1). The surface of the cylindrical receiver is formed with a number of smaller rectangular panels, each consisting of a number of vertical tubes filled with HTF that flows in parallel between a common lower and upper flow header, as shown in Fig. 3. The HTF enters the receiver from the north side, where the concentration of solar flux is maximum, and the temperature of the HTF is the lowest, and flows through one of the two 12-panel flow circuits as a serpentine flow, as shown in Fig. (3). The HTF then exits the system via the south side.

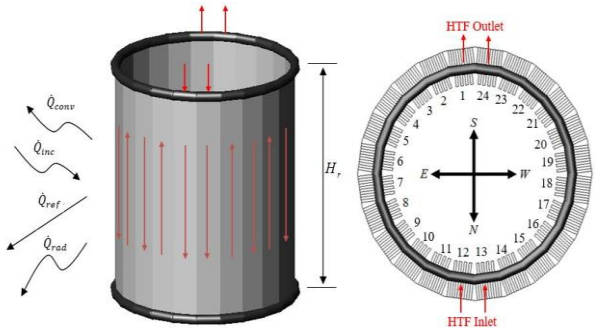

Fig. 3. Solar receiver with heat transfer losses

In addition, to maximize the absorption of the incident solar flux, the pipes are coated with high-absorptivity paint such as the black matte Pyromark™ paint used for Solar II and Gemasolar. According to the Gemasolar literature (Amadei 2013), the average absorptivity of this particular coating is claimed to be 95%, as presented in Table 1.

Receivers that use molten salt as the HTF are at an advantage because there is no phase change and it is possible to heat the HTF up to 595°C. For the receiver in the Gemasolar system, the HTF is a molten nitrate salt consisting of 60% $NaNO_3$ and 40% KNO_3 (Lata 2008), the properties of which are presented in (Ferri 2008). The HTF is pumped from the cold storage tank at 290°C into the receiver, where it is heated to 595°C and then pumped to

the hot storage tank (Amadei 2013). The mass flow rate of the HTF through the receiver is modulated to accommodate the desired outlet temperature from the tower as the incident flux varies throughout the procedure.

4.1 Shape distribution of the incident power on an external receiver

The scheme of the shape distribution of the incident power on the external receiver surface $\dot{Q}_{inc}(i,j)$ should be estimated before applying energy balance formulation, which can be done using analytic functions of the HFLCAL model (presented in section 2.1) with the adaptation projection model of Ref. (Sanchez 2015). Generally, the analytic functions of the HFLCAL model are estimated on the plane normal to the central reflected ray for each heliostat. Thus, the image plane is used in the projection method. First, discretize the receiver panels into several flux points per panel in the vertical direction, approximate them as much as possible into equilateral blocks. Then, divide each panel into nine blocks of the same length, after which the center of each discretization is projected onto the image plane in the direction of the central reflected ray, as shown in Fig. 4. Generally, the scale of resolution increases when the grid is more accurate; however, the computation time also increases.

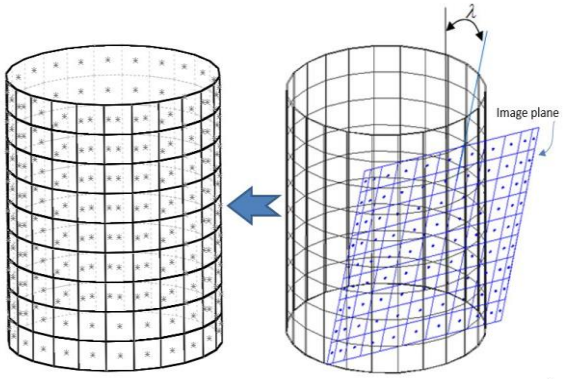

Fig. 4. Discretization of the surface of the solar receiver with present projection plane

For each heliostat in the field, we applied the analytic function in Ref. (Collado 2010), on the nodes in the image plane to estimate the shape distribution of the incident power, as given by Eq. (15).

$$\dot{Q}_{inc,h}(x_r,y_r)=\frac{E_b(t)\times A_m\times\eta_{ref}\times\eta_{cos}\times\eta_{at}\times\eta_{s\&b}}{2\pi\sigma_{tot}^2}e^{\left(-\frac{x_r^2+y_r^2}{2\sigma_{tot}^2}\right)}\ (w) \quad (15)$$

Next, the flux distribution is projected from the image plane to the receiver, the flux map caused by an entire field of heliostats is generated, and the shape distribution of the incident power at each center of the discretization element of the receiver $\dot{Q}_{inc}(i,j)$ is estimated, where i represent the number of panels n_p, and j represents the number of blocks n_b, which means that each block has its own incident power, as shown in Fig. (5), which clarify the $\dot{Q}_{inc}(i,j)$ at spring equinox-solar noon for Seville, Spain, that appear the close shape distribution with Ref. (Sanchez 2015) after comparison, and the total incident power equal at specified time, $\dot{Q}_{inc}=\sum_{i,j}\dot{Q}_{inc}(i,j)$

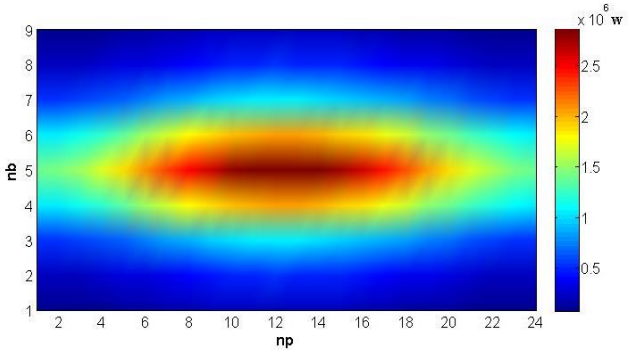

Fig. 5. Shape distribution of the incident power on the external surface at spring equinox-solar noon for Seville, Spain

The cylindrical surface of the external receiver is mapped to a planar surface in which the progression from 0° to 360° along the horizontal axis corresponds to the progression around the circumference of the receiver.
The maximum $\dot{Q}_{inc}(i,j)$ occurs at the northernmost panels where the angular position is 180°.

4.2 Energy balance and model formulation

The solar energy will be reflected by the heliostat field onto the receiver and absorbed by the HTF. The energy absorbed by the HTF would be the difference between the total incident energy and total losses through the receiver. These losses consist of 1) convective losses due to the air surrounding the receiver, which are directly related to local temperature and wind conditions; 2) radiative losses due to the radiations emitted from the receiver's hot surface to the environment; and 3) reflective losses due to the material's properties. These heat transfer losses are shown in Fig. 3.

The modeling tool is limited to the scheme of the $\dot{Q}_{inc}(i,j)$, which as estimated before contains one data point per panel in the circumferential direction and several flux points per panel in the vertical direction.

The proposed model considers that the inlet and outlet temperatures are fixed, that the tube-to-tube conduction and radiation exchange is negligible, and that the axial conduction is also small because the internal convection due to molten salt flowing in the tubes dominates the relatively large resistance to conduction.

The overall energy balance of the heat flow components entering and exiting each block in the receiver is expressed by Eq. (16) to estimate the absorbed heat $\dot{Q}_{\boldsymbol{abs}}(i,j)$:

$$\dot{Q}_{\boldsymbol{abs}}(i,j) = \dot{Q}_{inc}(i,j) - \left(\dot{Q}_{conv}(i,j) + \dot{Q}_{rad}(i,j) + \dot{Q}_{ref}(i,j)\right) (W) \quad (16)$$

Convective losses from different blocks,

$$\dot{Q}_{conv}(i,j) = \bar{h}_{mix}.A_{su}\left(T_{s,i,j} - T_{amb}\right) \quad (w) \quad (17)$$

The above result is obtained from forced and natural convection. The convection heat transfer coefficient can be estimated from the Eq. $\bar{h}_{mix} = \left(\bar{h}_{fc}^{3.2} - \bar{h}_{nc}^{3.2}\right)^{1/3.2}$ According to the correlations of Siebers and Kraabel, as presented in Ref. (Siebers 1984), where $\bar{h}_{fc}$ represents the forced convection coefficient, which is estimated from the Nusselt and Reynold numbers that are based on the receiver diameter and wind velocity, and $\bar{h}_{nc}$ is the natural convection coefficient, which is based on the Nusselt and Grashof numbers, that are consider the receiver height as characteristic length.

The radiation losses from different blocks are presented in Eqs. (18–20). The model of Ref. (Wagner 2008) considers the ambient air temperature and the effective sky temperature with suitable view factors in location between the receiver and temperature zones.

$$\dot{q}_{rad} = hr_{rad,amb} \cdot A_{su} \cdot \left(T_{s,i,j} - T_{amb}\right) + hr_{rad,sky} \cdot A_{su} \cdot \left(T_{s,i,j} + T_{sky}\right) \quad (W) \ (18)$$

$$hr_{rad,amb} = \sigma\varepsilon F_{s,amb}\left(T_{s,i,j}^2 + T_{amb}^2\right)\left(T_{s,i,j} + T_{amb}\right) \quad (W/m^2 \cdot k) \ (19)$$

$$hr_{rad,sky} = \sigma\varepsilon F_{s,sky}\left(T_{s,i,j}^2 + T_{sky}^2\right) \quad (W/m^2 \cdot k) \ (20)$$

The surface emissivity $= 0.88$, and the view factor between the ground and the tower and that between the sky and the tower are $F_{s,amb} = 0.5$ and $F_{s,sky} = 0.5$, respectively. The sky temperature is as shown in Eq. (21) from Ref. (ASHRAE 2011).

$$T_{sky} = 0.0552T_{amb}^{1.5} \quad (k) \quad (21)$$

The reflection is as shown in Eq. (22)

$$\dot{Q}_{ref}(i,j) = (1 - 0.95).\dot{Q}_{inc}(i,j) \quad (w) \quad (22)$$

The surface area A_{su} of the element equals $n_t(\pi r_o L)$, where L is the length of the panel block in the vertical direction, and r_o, r_1 are the absorber tube's inner and outer radii, respectively.

4.3 Temperatures of receiver surface and HTF for each block

The first consideration in the computation of heat losses is the calculation of the average receiver surface and HTF temperatures for each block because they are required for almost all types of heat loss computations, excluding reflective heat loss. To determine the temperatures of the HTF along the flow path of the HTF through the receiver tubes, as shown in equation (23), which depend on the accumulated heat from the entrance until the block where the temperature of the HTF is computed, that mean, as mentioned before the HTF flow in two paths in the receiver, each path flow in 12 panels and 9 blocks in each panel, each path consist of 108 blocks, then to simplified computations, defined length of path flow (L_{pf}) Which present the sequence of the blocks with path flow, then when computed temperature for specified block, should estimate the summation heat for all heat from entrance to specify a block, as Consecutively to the fluid flow path, or in the other ward, follow the flow of the HTF as shown in Fig. (3), that mean the sequence of the summation in Eq. (23) for the specified number of (L_{pf}), start from the first element in panel 12 and end at (n=108), for path flow (north-east- south) and the sequence of the number of the elements (i,j) That corresponding to the sequence of the length of the path flow of HTM, and for other path start from the first element in panel 13 and end at (n=108), for path flow (north-west south), and same procedure for sequence of blocks.

$$T_{\mathrm{HTF}}(i,j) = T_{\mathrm{HTF}}\left(L_{pf}\right) = 290 + \sum_{L_{pf}=1}^{n} \frac{\dot{Q}_{\boldsymbol{absorb}}(i,j)}{\dot{m}_{\mathrm{HTF,p}}.cp_{\mathrm{HTF}}} \quad (23)$$

$\dot{m}_{\mathrm{HTF,p}}$ represents the mass flow rate of the HTF for each panel, and $T_{\mathrm{HTF}}(0)$ equals 290 °C, which is the entrance temperature for the HTF

Further, an additional energy balance is required to estimate the surface temperature of the element $T_{s,i,j}$. This balance considers the thermal resistance between the outer surface of the tube and the HTF running through the tube, and can be described by Eq. (24):

$$T_{s,i,j} = \frac{\dot{Q}_{\boldsymbol{abs}}(i,j)}{n_t}\left(\frac{ln(r_o/r_i)}{2\pi Lk} + \frac{1}{h_{in}(2\pi r_i L)}\right) + T_{\mathrm{HTF}}(i,j) \quad (24)$$

where $T_{\mathrm{HTF}}(i,j)$ is the HTF temperature in the absorber tube. In this case, the tube material is a nickel alloy (800H) (Amadei 2013).

In Eq. (24), h_{in} is the HTF convective heat transfer coefficient in the absorber tube. The classical Dittus–Boelter equation presented in (Li 2010) is applied in Eq. (25):

$$Nu_{ms} = 0.023Re^{0.8}Pr^{0.4} \quad (25)$$

This mathematical model is further refined by two more steps. First, the $T_{\mathrm{HTF}}(i,j)$ and $T_{s,i,j}$ temperatures are calculated beginning with a set of values based on the conjecture that is then adjusted through iteration. The main assumption used to start this calculation is that $\sum_{i,j} \dot{Q}_{\boldsymbol{abs}}(i,j) = \sum_{i,j} \dot{Q}_{inc}(i,j)$, after which the mass flowrate for each path flow $\dot{m}_{\mathrm{HTF,p}}$ is esimated. Then, the temperature $T_{\mathrm{HTF}}(i,j)$ along path flow of the HTF from Eq. (23) with an initial estimation of the fluid property is estimated, after which $T_{s,i,j}$ is estimated from Eq. (24).

Second, $T_{s,i,j}$ is substituted in heat losses equations (17–22) to determine $\dot{Q}_{\boldsymbol{abs}}(i,j)$ from Eq. (16), and then $T_{\mathrm{HTF}}(i,j)$ and $T_{s,i,j}$ are recalculated using the new $\dot{Q}_{\boldsymbol{abs}}(i,j)$ value. Subsequent $\dot{Q}_{\boldsymbol{abs}}(i,j)$ values are compared, and if the difference is equal to 0.001, the last value can be considered the true value, this computation and comparison occur for each element, with consider the path of HTF flow, then the last comparison will be for the total value $\sum_{i,j} \dot{Q}_{\boldsymbol{abs}}(i,j)$ with same difference and the last value can be considered the true value.

Finally, to validate a thermal model for the solar receiver, we compare the efficiency value at spring equinox-solar noon in Seville, Spain, with the experimental result of Ref. (Pacheco 2002), considering the same condition and selecting the highest wind speed in the reference 6.4 m/s. The reference result is 85.6%, and the result in the present model result is 87.904%.

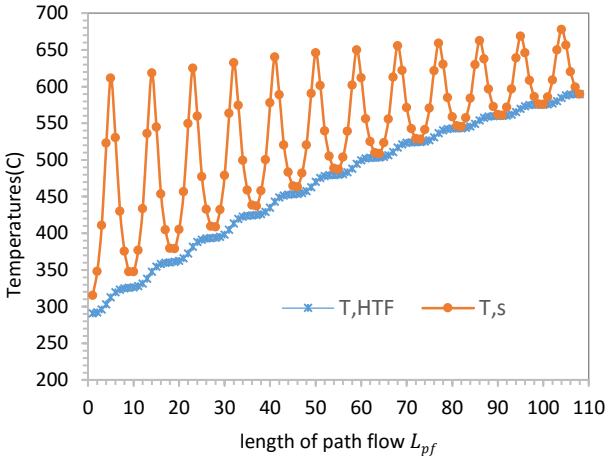

Fig. 6. Temperatures of $T_{\mathrm{HTF}}(i,j)$ and $T_{s,i,j}$ along length of path flow L_{pf}

By using another validation, the result shows the convergence with one of the results of Ref. (Lata 2008) for different models of the receiver, who show an efficiency range of different model (77.4%–87.6%) and the last validation by estimate the distribution of the temperatures $T_{\mathrm{HTF}}(i,j)$, and $T_{s,i,j}$ along the path flow of HTF which presented in Fig. (6) That appears close to result of Ref. (Gregory 2011).

5. Result of Analysis of simulating the SPTP behavior in different locations

Our main objective was to study the potential of concentrating solar power by SPTPs in new areas such as the south of Turkey (Gaziantep, Sanliurfa, and Finike), in addition to existing locations such as Gemasolar in Seville, Spain. The analysis focused on three energy conditions: the SPTPs input solar radiation $E_b(t)$, the output energy from the heliostat field $\dot{Q}_{inc}(t)$, and the output energy from the solar receiver $\dot{Q}_{\boldsymbol{abs}}(t)$. A dynamic simulation developed in MATLAB was structured to focus on the performance of the heliostat field and solar receiver because these units are the parts of the plant that are most affected by the location conditions, including solar radiation, ambient temperature, latitude and longitude angles, and wind speed. In addition, the daily accumulated energy results for the 21st day of each month, from sunrise to sunset, were determined for each unit to clearly understand the SPTP unit's performance at each hypothetical location. The first location represents the original location of Gemasolar in Seville, Spain (Lat. 37.42N), which was considered as the reference in this study. Fig. 7 presents the accumulated input and output energies for the heliostat field and receiver for 12 average days.

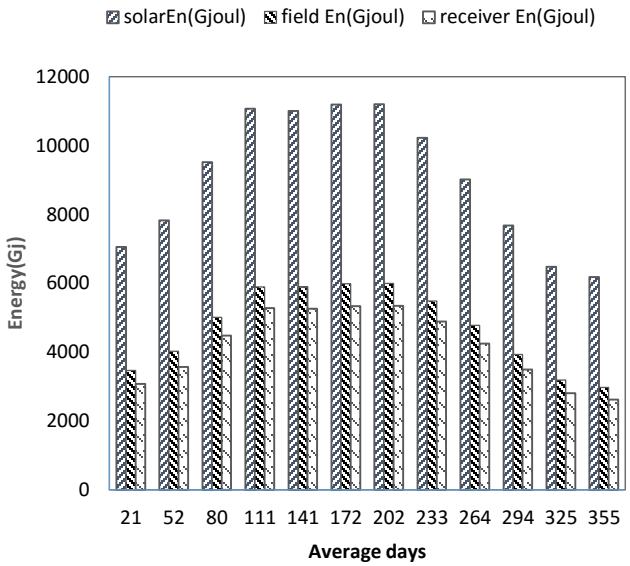

Fig. 7. Accumulated solar energies transformed from the heliostat field and receiver for 12 average days in Seville, Spain

Figs. 8–10 present the accumulated input and output energies from the heliostat field and receiver for 12 average days at three other locations in the south of Turkey (Gaziantep, Sanliurfa, and Finike).

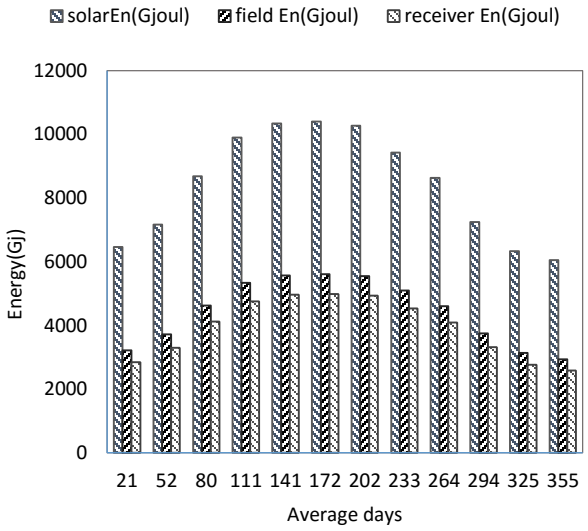

Fig. 8. Accumulated energies for Gaziantep, Turkey

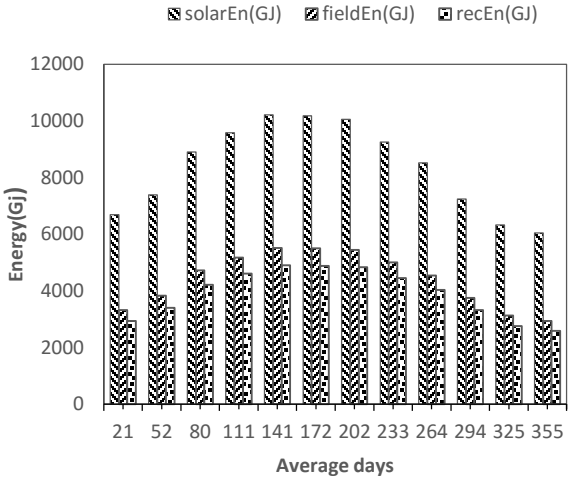

Fig. 9. Accumulated energies for Sanliurfa, Turkey

For all locations, the total field and receiver efficiencies with the number of days which have maximum and minimum values for the accumulated solar energies are as shown in Table 3. Finally, as we have already noted, the main reference Gemasolar in Seville, Spain, exhibits the best SPTP potential energies. With regard to the other selected cities in Turkey, the results show that the SPTP will exhibit the best performance in Gaziantep, as shown in the previous figures and in Fig. 12, which presents the total accumulated solar energies for all 12 days for each different location. For all the cities in Turkey, the results are close in terms of field efficiency the lowest field efficiency value was exhibited in Seville, Spain, and the lowest receiver efficiency was exhibited in Finike ; however, this SPTP in Seville exhibits the highest receiver efficiency value with the highest solar radiation, and Seville is therefore the best SPTP location investigated in this study.

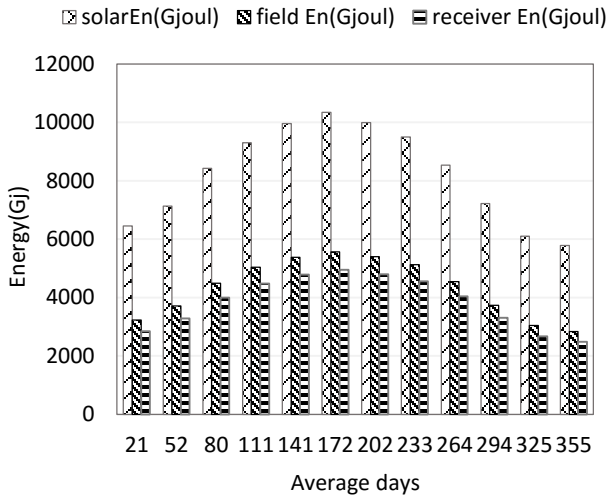

Fig. 10. Accumulated energies for Finike, Turkey

6. Conclusion

The performance was compared based on the cumulative energies of the units under investigation, using Gemasolar as a reference. A comparison of these results showed that among the accumulated energies of the heliostat field and receiver for areas in the south of Turkey (Gaziantep, Sanliurfa, and Finike), the highest accumulated energy was exhibited in Gaziantep, after the reference location in Seville, Spain, and the minimum accumulated energy was exhibited in Finike, Turkey. On the other hand, the field efficiency for all locations tested in Turkey is equal or higher than the reference location. Further, the highest value for receiver performance occurred in Seville, Spain, compared to the values in Gaziantep and Sanliurfa, and the minimum value occurred in Finike, Turkey. Further, the result shows that the highest net output energy in Turkey (Gaziantep) was less than the reference case by about 6.71%.

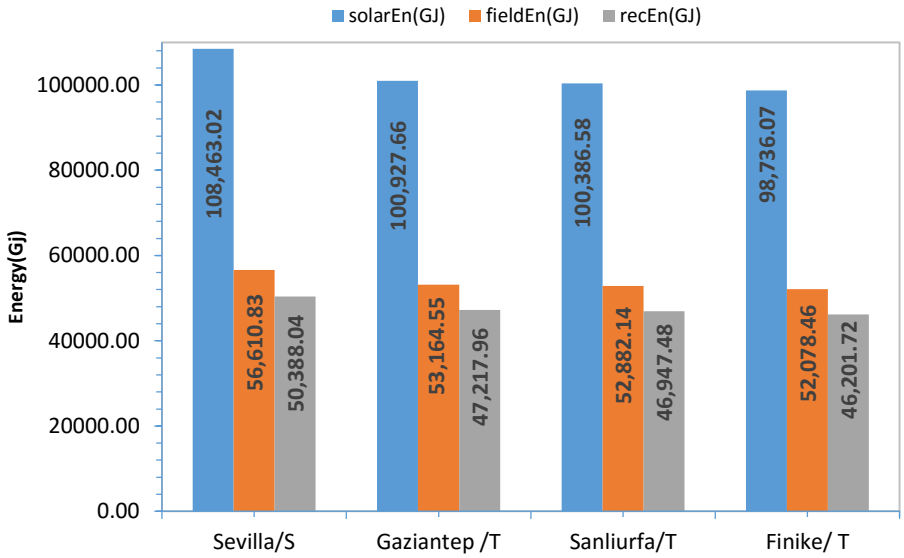

Fig. 12. Total accumulated solar energies for all 12 days at different locations

Table 3.
Properties for each city

Location	Seville, Spain	Gaziantep, Turkey	Sanliurfa, Turkey	Finike, Turkey
Field efficiency	0.529	0.534	0.534	0.534
Receiver efficiency	0.890	0.888	0.888	0.887
Day number that has maximum energies	202	172	141	172
Day number that has minimum energies	355	355	355	355

Abbreviations

ASHRAE : American Society of Heating, Refrigeration, and Air-condition Engineers
DB : Dry bulb
HTF : Heat transfer fluid
MCDBR : Mean daily DB temperature range
SPTP : Solar power tower plant

References

American Society of Heating, Refrigerating, and Air-Conditioning Engineers (ASHRAE), 2011 ASHRAE Handbook—HVAC Applications (SI).

American Society of Heating, Refrigerating, and Air-Conditioning Engineers (ASHRAE), 2013 ASHRAE Handbook - Fundamentals (SI); Climatic Design Information, ASHRAE, Georgia, USA, 2013.

Amadei, C.A., Allesina, G., Tartarini, P., Yuting, W. (2013) Simulation of GEMASOLAR-based solar tower plants for the Chinese energy market: influence of plant downsizing and location change. Renewable Energy, 55,366–373.

Burgaleta, J.I., Arias, S., Ramirez, D. (2011) GEMASOLAR: the first tower thermo-solar commercial plant with molten salt storage. SolarPA-CES 2012 International Conference.

Besarati, S.M., Goswami, D.Y. (2014) A computationally efficient method for the design of the heliostat field for solar power tower plant. Renewable Energy, 69, 226–232.

Collado, F.J. (2010) One-point fitting of the flux density produced by a heliostat. Solar Energy, 84, 673–684.

Chong, K.K., Tan, M.H. (2011) Range of motion study for two different sun-tracking methods in the application of heliostat field. Solar Energy, 85, 1837–1850.

Collado, F.J., Guallar, J. (2012) Campo: generation of regular heliostat fields. Renewable Energy, 46,49–59.

Collado, F.J., Guallar, J. (2013) A review of optimized design layouts for solar power tower plants with campo code. Renewable Sustainable Energy Review, 20, 142–154.

Chiesi, M., Vanzolini, L., Scarselli, E.F., Guerrieri, R. (2013) Accurate optical model for design and analysis of solar fields based on heterogeneous multicore systems. Renewable Energy, 55, 241-251.

Duffie J.A., Beckman W.A. (1991) Solar engineering of thermal processes. New York: Wiley.

Ferri, R., Cammi, A., Mazzei, D. (2008) Molten salt mixture properties in RELAP5 code for thermodynamic solar

applications. International Journal of Thermal Science, 47, 1676–1687.

Garcia, P., Ferriere, A., Bezian, J.-J. (2008) Codes for solar flux calculation dedicated to central receiver system applications: a comparative review. SolAR Energy 82: 189–197.

Gregory J. K. An Evaluation of Possible Next-Generation High-Temperature Molten-Salt Power Towers. Sandia National Laboratories, SAND2011-9320 Albuquerque, NM.

Kolb, G.J., Ho, C.K., Mancini, T.R., Gary, J.A. (2011) Power tower technology roadmap and cost reduction plan. SAND2011-2419, Alburquerque 1–35.

Lata, J.M., Rodríguez, M., Álvarez de Lara, M. (2008) High flux central receivers of molten salts for the new generation of commercial stand-alone solar power plan. Journal of Solar Energy Engineering, 130, 021002.

Li, X., Kong, W., Wang, Z., Chang, C., Bai, F. (2010) Thermal model and thermodynamic performance of molten salt cavity receiver, Renewable Energy, 35, 981–988.

Leonardi, E, D'Aguanno, B. (2011) CRS4-2: a numerical code for the calculation of the solar power collected in a central receiver system. Energy, 36, 4828–4837.

Noone, C.J., Torrilhon, M., Mitsos, A. (2012) Heliostat field optimization: a new computationally efficient model and biomimetic layout. Solar Energy, 86, 792–803.

Pacheco, James E. Final Test and Evaluation Results from the Solar Two Project. SAND2002-0120. Sandia National Laboratories, Albuquerque, NM.

Siebers, D.L., Kraabel, J.S. (1984) Estimating Convective Energy Losses from Solar Central Receivers. Sandia National Laboratories, Albuquerque. SAND 84-8717.

Stine, W.B., Harrigon, R.W. (1985) Solar Energy Fundamentals and Design with Computer Application. New York: Wiley.

Siala, F.M.F., Elayeb, M.E. (2001) Mathematical formulation of a graphical method for a no-blocking heliostat field layout. Renewable Energy, 23, 77–92.

Schmitz, M., Schwarzbozl, P., Buck, R., Pitz-Paal R. (2006). Assessment of the potential improvement due to multiple apertures in central receiver systems with secondary concentrators. Solar Energy, 80,111–120.

Sanchez-Gonzalez, A., Santana, D. (2015) Solar flux distribution on central receivers: A projection method from analytic function. Renewable Energy, 74, 576–587.

Wagner, M.J. (2008) Simulation and predictive performance modeling of utility-scale central receiver system power plant. Thesis, University of Wisconsin-Madison, Wisconsin, USA.

Wei, X., Lu, Z., Yu, W., Wang, Z. (2010) A new code for the design and analysis of the heliostat field layout for power tower system. Solar Energy, 84, 685–690.